Communications in Physics, Vol. 34, No. 4 (2024), pp. 351-363
DOI: https://doi.org/10.15625/0868-3166/21530

Influence of third-order susceptibility on electromagnetically induced grating in a three-level V-type atomic system

Nguyen Huy Bang[1], **Dinh Xuan Khoa**[1], **Luong Thi Yen Nga**[1], **Ho Hai Quang**[1], **Nguyen Van Ai**[2] **and Le Van Doai**[1,†]

[1]*Vinh University, 182 Le Duan Street, Vinh City, Vietnam*
[2]*Ha Tinh University, 26/3 Street, Ha Tinh City, Vietnam*

E-mail: †doailv@vinhuni.edu.vn

Received 18 September 2024
Accepted for publication 6 December 2024
Published 15 December 2024

Abstract. *In addition to the suppressed absorption in the atomic resonance region, an electromagnetically induced transparency (EIT) medium also possesses giant nonlinear dispersion which significantly affects the optical properties of the medium. In this work, we study the influence of third-order nonlinear susceptibility on electromagnetically induced grating (EIG) in a three-level V-type atomic medium. By applying stationary perturbation theory to the density matrix equations describing the time evolution of the quantum states of the system, we have found density matrix solutions to the third-order perturbation corresponding to the third-order susceptibility, and found the transmission function for the probe light. Using the Fourier transform of the transmission function, we can obtain the intensity distribution function of the EIG diffraction spectrum as a function of laser parameters and the atomic medium. To see the influence of third-order susceptibility on EIG diffraction spectrum, we have simulated EIG spectra in two cases with and without third-order susceptibility. We found that the first-order diffraction efficiency was significantly enhanced when third-order susceptibility was introduced.*

Keywords: effects of atomic coherence; diffraction grating.
Classification numbers: 42.50.Gy; 42.65.-k.

1. Introduction

Diffraction grating is commonly used as dispersive elements in many optical systems for applications including spectrometers, switching, tuning and trimming elements in dense wavelength-division multiplexing, visual display technology, external cavity lasers, etc., [1]. In such applications, high first-order diffraction efficiency is always desired since it will strongly influence the final energy delivered by the optical diffraction system. However, for a given grating it is very difficult to change the high-order diffraction efficiency.

The coherent interaction between the laser fields with the atom can lead to a quantum interference of transition probabilities within the atomic system. As a result, it suppresses (destructive interference) or enhances (constructive interference) the total transition probability and thus significantly changes the absorption or transmission property of the atomic medium for a light field. The constructive interference of transition probabilities can generate electromagnetically induced transparency (EIT) [2], while the destructive interference can lead to electromagnetically induced absorption (EIA) [3]. Thus, the basic configuration of the EIT effect is three-level quantum systems that are excited by a probe laser field and a coupling laser field. In the presence of the coupling beam, the probe beam can be completely transmitted through the atomic medium. Therefore, if the coupling beam is a standing wave field with nodes and antinodes, it will cause in space a periodic modulation of the transmitted spectrum of the probe field. This means that the probe field propagates through the atomic medium just as it passes through a diffraction grating which is called electromagnetically induced grating (EIG) and the probe field can be diffracted into the high-order directions [4]. EIG was first proposed in 1998 [4] and experimentally verified in 1999 [5]. Since then, theoretical and experimental studies of EIG have attracted great attentions [6–9] due to their potential applications in many fields, such as atoms velocimetry [10], light storage [11], beam splitting and fanning [12], shaping a biphoton spectrum [13], controlling multi-wave mixing processes [14], angular Talbot effect [15] and giant Goos-Hänchen shifts [16]. Recently, EIG efficiency has been greatly improved with the support of other external fields such as microwave field [17] and magnetic field [18] as well as coherence effects such as coherent population trapping (CPT) [19] and spontaneously generated coherence (SGC) [20].

In addition to dramatic reduction of light absorption in the atomic resonance region, the EIT medium also possesses a giant Kerr nonlinearity. Indeed, Wang *et al.*, have experimentally demonstrated that the nonlinearity can be enhanced by millions of times in the presence of EIT [21]. Therefore, the applied studies of EIT medium need to consider the influence of nonlinearity on the optical response of the atomic medium. For example, the group index can be larger when the Kerr nonlinearity is included [22, 23]. Likewise, the diffraction efficiency of EIG can be improved in the presence of Kerr nonlinearity [19, 20, 24]. For instance, in Ref. [24] the authors added a Kerr field to create a cross-Kerr effect and demonstrated that the higher order diffraction intensity of the probe beam increases under the Kerr field.

In this work, we study the formation of the diffraction pattern of EIG in a three-level V-type atomic system in the presence of self-Kerr nonlinearity. Unlike the work [24], here we consider the self-Kerr effect of the probe field itself without introducing the additional Kerr field. The influence of the intensity and frequency of the laser fields on the diffraction pattern of EIG were also investigated.

2. Theoretical model

Figure 1(a) shows a three-level V-type atomic system excited by probe and coupling fields, in which, the transition $|1\rangle \leftrightarrow |2\rangle$ is driven by a weak probe field E_p with an angular frequency ω_p, while the transition $|1\rangle \leftrightarrow |3\rangle$ is coupled by a strong coupling field E_c with an angular frequency ω_c. Spontaneous decay rates from levels $|2\rangle$ and $|3\rangle$ to level $|1\rangle$ are Γ_{21} and Γ_{31}, respectively, while Γ_{32} is the relaxation rate between the excited states $|2\rangle$ and $|3\rangle$ by collisions. We denote $\Delta_p = \omega_p - \omega_{21}$ and $\Delta_c = \omega_c - \omega_{31}$ are the frequency detunings of the probe and coupling fields from the atomic transition frequencies, respectively. The Rabi frequencies of the probe and coupling fields are respectively given by $\Omega_p = d_{21}E_p/\hbar$ and $\Omega_c = d_{31}E_c/\hbar$ with d_{mn} being the electric-dipole matrix element associated with the transition from the state $|m\rangle$ to the state $|n\rangle$.

We assume that the probe field is travelling wave propagating along the z-direction and is represented by $\varepsilon_p = \frac{1}{2}E_p e^{-i\omega_p t + ik_p z} + c.c.$, where E_p is assumed to be unchanged along the x-direction and the wave vector with is the wavelength of the probe laser field. Meanwhile, the coupling field is the standing wave and is expressed by $\varepsilon_c = \frac{1}{2}E_c \sin(k_{cx}x)e^{-i\omega_c t + ik_{cz}z} + c.c.$, where E_c is taken as the constant amplitude factor, and the wave vector $k_p = 2\pi/\lambda_p$ with λ_p can be written as $k_{cx} = \frac{2\pi \sin\phi}{\lambda_c} \equiv \frac{\pi}{\Lambda}$ and $\Lambda = \frac{\lambda_c}{2\sin\phi}$, λ_c is the wavelength of the coupling field and ϕ is the angle made by the direction of the coupling field to the direction of the probe field propagating towards the z-axis. Where, Λ denotes the separation between two consecutive nodes, or antinodes. By changing the angle ϕ the value of Λ can be varied. Fig. 1(b) shows the probe and coupling laser propagations through the atomic medium.

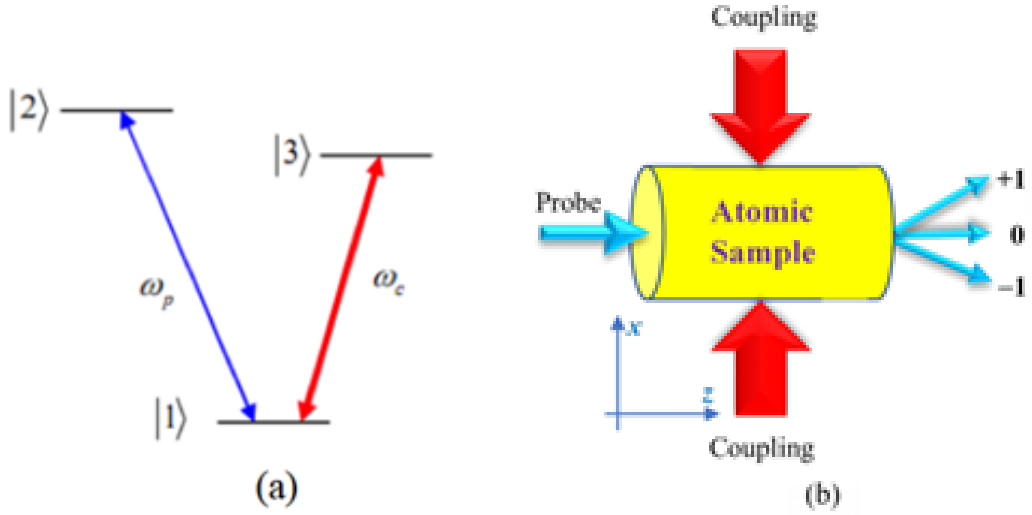

Fig. 1. (a) The excited scheme of three-level V-type atomic system. (b) Orientations of probe and coupling laser fields propagating through the atomic medium.

The time evolution of atomic states in laser fields which are represented by the density matrix ρ is obeyed by the following Liouville equation [25]:

$$\dot{\rho} = -\frac{i}{\hbar}[H,\rho] + \Gamma\rho, \tag{1}$$

where the term $\Gamma\rho$ presents the relaxation mechanisms of system. Total Hamiltonian H is the sum of the unperturbed atomic Hamiltonian H_{at} and the interaction Hamiltonian H_{int}, is given by [4]:

$$H = \sum_{n=1}^{3} \hbar\omega_n |n\rangle\langle n| + \Omega_p e^{-i\omega_p t + ik_p z} |1\rangle\langle 2| + \Omega_{0c} \sin\left(\frac{\pi x}{\Lambda}\right) e^{-i\omega_c t + ik_{cz} z} |1\rangle\langle 3| + c.\text{c}, \tag{2}$$

where, $\Omega_p = d_{21}E_p/\hbar$ and $\Omega_{0c} = d_{31}E_c/\hbar$ are Rabi frequencies induced by the probe and coupling laser fields, respectively.

Using electric-dipole and rotating-wave approximations, the density matrix equations representing the atomic population and coherence are expressed as [3]:

$$\dot{\rho}_{11} = \Gamma_{21}\rho_{22} + \Gamma_{31}\rho_{33} + \frac{i}{2}\Omega_p(\rho_{21} - \rho_{12}) + \frac{i}{2}\Omega_c(\rho_{31} - \rho_{13}), \tag{3}$$

$$\dot{\rho}_{22} = -\Gamma_{21}\rho_{22} - \Gamma_{23}\rho_{33} + \frac{i}{2}\Omega_p(\rho_{12} - \rho_{21}), \tag{4}$$

$$\dot{\rho}_{33} = -\Gamma_{31}\rho_{33} + \Gamma_{23}\rho_{22} + \frac{i}{2}\Omega_c \sin\left(\frac{\pi x}{\Lambda}\right)(\rho_{13} - \rho_{31}), \tag{5}$$

$$\dot{\rho}_{31} = (i\Delta_c - \gamma_{31})\rho_{31} - \frac{i}{2}\Omega_p\rho_{32} + \frac{i}{2}\Omega_c \sin\left(\frac{\pi x}{\Lambda}\right)(\rho_{11} - \rho_{33}), \tag{6}$$

$$\dot{\rho}_{23} = [i(\Delta_c - \Delta_p) - \gamma_{23}]\rho_{23} + \frac{i}{2}\Omega_p\rho_{13} - \frac{i}{2}\Omega_c \sin\left(\frac{\pi x}{\Lambda}\right)\rho_{21}, \tag{7}$$

$$\dot{\rho}_{21} = (i\Delta_p - \gamma_{21})\rho_{21} - \frac{i}{2}\Omega_c \sin\left(\frac{\pi x}{\Lambda}\right)\rho_{23} + \frac{i}{2}\Omega_p(\rho_{11} - \rho_{33}), \tag{8}$$

$$\rho_{nm} = \rho^*_{mn} \tag{9}$$

$$\rho_{11} + \rho_{22} + \rho_{33} = 1. \tag{10}$$

Here γ_{mn} is the dephasing rate of atomic coherence ρ_{mn} which is related to the spontaneous decay rate γ_{mn} as follows:

$$\gamma_{mn} = \frac{1}{2}\left(\Sigma_{k<m}\Gamma_{mk} + \Sigma_{l<n}\Gamma_{nl}\right). \tag{11}$$

In order to investigate the linear and nonlinear optical properties of the medium, we need to derive the expressions for the linear and nonlinear susceptibilities by finding the solution for density matrix elements up to third-order perturbation (under the steady-state condition) via an iterative technique. That is, the density matrix elements can be expanded as [21]:

$$\rho_{mn} = \rho^{(0)}_{mn} + \rho^{(1)}_{mn} + \cdots \rho^{(n)}_{mn}. \tag{12}$$

Assuming that initially, the population is in the ground state $|1\rangle$, $\rho^{(0)}_{11} \approx 1$, while $\rho^{(0)}_{22} \approx \rho^{(0)}_{33} \approx 0$. In the weak-field approximation of the probe light, we find the solution for the density matrix ρ_{21} from Eqs. (3), in the first-order perturbation as

$$\rho^{(1)}_{21} = \frac{\frac{i}{2}\Omega_p(\rho^{(0)}_{11} - \rho^{(0)}_{22})}{\gamma_{21} - i\Delta_p + \frac{(\Omega_c/2)^2 \sin^2\left(\frac{\pi x}{\Lambda}\right)}{\gamma_{23} - i(\Delta_p - \Delta_c)}} \approx \frac{i\Omega_p}{2F} \tag{13}$$

where

$$F = \gamma_{21} - i\Delta_p + \frac{(\Omega_c/2)^2 \sin^2\left(\frac{\pi x}{\Lambda}\right)}{\gamma_{23} - i(\Delta_p - \Delta_c)} \tag{14}$$

In a similar way, we can be found the expression for ρ_{21} in third-order as

$$\rho_{21}^{(3)} = \frac{\Omega_p^2}{2\Gamma_{21}} \frac{i\Omega_p}{F} \left[\frac{1}{F} + \frac{1}{F^*} \right]. \tag{15}$$

Finally, the density matrix element ρ_{21} up to third-order can be obtained as

$$\rho_{21} = \rho_{21}^{(1)} + \rho_{21}^{(3)} = \frac{-i\Omega_p}{2F} + \frac{i\Omega_p}{2F} \frac{\Omega_p^2}{\Gamma_{21}} \left(\frac{1}{F} + \frac{1}{F^*} \right). \tag{16}$$

Here $F^\star$ is the complex conjugation of F.

The probe susceptibility *chi* is proportional to ρ_{21} as follows

$$\chi = 2\frac{Nd_{21}}{\varepsilon_0 E_p} \rho_{21} \equiv \frac{Nd_{21}}{\varepsilon_0 E_p} \left[\frac{i\Omega_p}{2F} - \frac{i\Omega_p}{2F} \frac{\Omega_p^2}{\Gamma_{21}} \left(\frac{1}{F} + \frac{1}{F^*} \right) \right]. \tag{17}$$

Here N is the atomic number density in the medium and ε_0 is vacuum permittivity.

On the other hand, the probe susceptibility can be presented in an alternative form as

$$\chi = \chi^{(1)} + 3E_p^2 \chi^{(3)}. \tag{18}$$

From Eqs. (17) and (18) we can extract the first-order susceptibility and the third-order susceptibility as follows

$$\chi^{(1)} = \frac{Nd_{21}^2}{\varepsilon_0 \hbar} \left(\frac{A}{A^2+B^2} + i\frac{B}{A^2+B^2} \right), \tag{19}$$

$$\chi^{(3)} = -\frac{Nd_{21}^4}{3\varepsilon_0 \hbar^3} \frac{1}{\Gamma_{21}} \frac{B}{A^2+B^2} \left(\frac{A}{A^2+B^2} + i\frac{B}{A^2+B^2} \right), \tag{20}$$

where A and B are controllable parameters that determined by

$$A = -\Delta_p + \frac{(\Delta_p - \Delta_c)}{\gamma_{23}^2 + (\Delta_p - \Delta_c)^2} \left(\frac{\Omega_c}{2} \sin\left(\frac{\pi x}{\Lambda} \right) \right)^2, \tag{21}$$

$$B = \gamma_{21} + \frac{\gamma_{23}}{\gamma_{23}^2 + (\Delta_p - \Delta_c)^2} \left(\frac{\Omega_c}{2} \sin\left(\frac{\pi x}{\Lambda} \right) \right)^2. \tag{22}$$

In order to describe the diffraction pattern of the probe field in the medium, we begin with the Maxwell equation. It is supposed that the probe field is propagating along the z direction through an atomic sample of length L. In the slowly varying envelope approximation, the Maxwell equation with the atomic polarization as:

$$\frac{\partial \varepsilon_p}{\partial z} = i\frac{\pi}{\varepsilon_0 \lambda_p} P, \tag{23}$$

Using the expression of polarization, therefore, Eq. (23) can be written as:

$$\frac{\partial \varepsilon_p}{\partial z'} = i\chi \varepsilon_p, \tag{24}$$

where $z' = (\pi N d_{21}^2 / 2\varepsilon_0 \hbar \lambda_p) z$ and z' can be made dimensionless when $z_0 = 2\varepsilon_0 \hbar \lambda_p / \pi N d_{21}^2$ is taken as the unit for z. If we consider z to be the effective length L traversed by the probe field through the medium, then the normalized transmission function can be written as [7]:

$$T(x) = e^{-\mathrm{Im}(\chi)L} e^{i\mathrm{Re}(\chi)L}, \tag{25}$$

where the terms $e^{-\mathrm{Im}(\chi)L}$ and $e^{i\mathrm{Re}(\chi)L}$ are associated with absorption and phase modulations, respectively. Because of the existence of the standing wave coupling field, the transmission function for the probe field is spatially modulated. The Fraunhofer diffraction equation can be obtained by the Fourier transformation of $T(x)$ [7]:

$$I_p(\theta) = |F(\theta)|^2 \frac{\sin^2(M\pi \sin(\theta) R)}{M^2 \sin^2(\pi \sin(\theta) R)}, \tag{26}$$

$$F(\theta) = \int_0^1 T(x) \exp(-2i\pi x . \sin(\theta) R) dx, \tag{27}$$

where $R = \Lambda / \Lambda_p$, the angle θ is the diffraction angle of the probe field regarding the z direction, and the parameter M is introduced as the spatial width of the probe beam.

3. Results and discussion

In the graphical examinations, we apply the theoretical model to the ^{85}Rb atom with the following states $|1\rangle = |5S_{1/2}, F = 1\rangle$, $|2\rangle = |5P_{3/2}, F' = 2\rangle$ and $|3\rangle = |5P_{1/2}, F' = 2\rangle$. The atomic parameters are given by: $\gamma_{21} = 5.6$ MHz, $\gamma_{23} = 6.0$ MHz, and $d_{21} = 1.6 \times 10^{-29}$ C.m. For simplicity, all quantities related to frequency are given in units γ which should be in the order of MHz for the rubidium atom.

In Fig. 2, we simulate the probe absorption of the three-level V-type atomic medium in the presence and absence of the third-order susceptibility. The laser parameters used in Fig. 2 as $\omega_p = 1\gamma$, $\omega_c = 30\gamma$ and $\Delta_p = \Delta_c = 0$. We can observe from Fig. 2 that, with coupling laser intensity $\omega_c = 30\gamma$, an EIT window with approximately 100% efficiency appears at the resonant probe frequency $\Delta_p = 0$. However, the presence of the third-order susceptibility ($\chi^{(3)}$) causes the absorption peaks on both sides of the EIT window to be significantly reduced (see solid line). This can be explained based on expressions (19) and (20) that the third-order susceptibility is of opposite sign to the first-order susceptibility, so when the third-order susceptibility is included, the amplitude of the probe absorption (the imaginary part of the total susceptibility) is reduced.

In Fig. 3, we replace the traveling wave coupling field by the standing-wave field and simulate the transmission function of the probe field $|T(x)|$ with respect to position x (in units of Λ). The laser parameters used in Fig. 3 as $\omega_p = 1\gamma$, $\omega_c = 30\gamma$, $\Delta_p = \Delta_c = 0$, M = 7, L = 15 and R = 4. It can be seen that the transmission spectrum of the probe field (cw) varies periodically in space; at the node positions of the standing-wave field (in this case, $x = 0, \pm 4, \pm 8$) the probe absorption is maximum (and hence no light signal is transmitted through the atomic medium), whereas at antinode positions ($x = \pm 2, \pm 6$) the probe light field becomes transparent to the medium (i.e., it is completely transmitted). Therefore, the probe field propagates through the atomic medium just as it passes through a diffraction grating and the transmitted probe field can be diffracted.

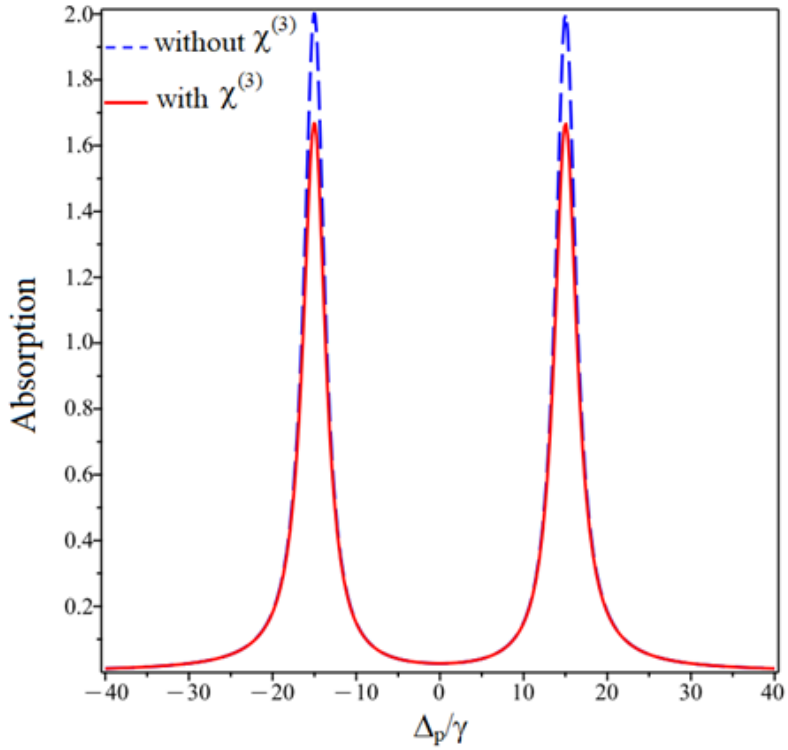

Fig. 2. Probe absorption Im(χ) without $\chi^{(3)}$ (dashed line) and with $\chi^{(3)}$ (solid line) at the laser parameters as $\omega_p = 1\gamma$, $\omega_c = 30\gamma$ and $\Delta_c = \Delta_p = 0$.

Now, we simulate the Fraunhofer diffraction pattern of the probe beam in the case with and without the third-order susceptibility at the parameters M = 7, L = 15, R = 4, ω_p = 1γ, ω_c = 30γ and Δ_p = Δ_c = 0, as shown in Fig. 4. It can be observed from Fig. 4 that the zero-order, first-order and second-order diffractions are localized at sinθ = 0, sinθ = ±0.25 and sinθ = ±0.5, respectively; the most of the light energy is distributed at the central maximum (zero-order diffraction). In fact, in the EIT spectral domain both absorption and dispersion are zero, so the Fraunhofer diffraction pattern of the probe beam is formed based on the amplitude modulation of the transmission function which tends to accumulate energy into the central diffraction maximum. On the other hand, by comparing the solid and dashed lines in Fig. 4 we see that in the presence of the third-order susceptibility, the diffraction efficiency is also increased (see solid line) which is consistent with the absorption spectrum in Fig. 2.

In Figs. 5 and 7, we consider the influence of the coupling and probe frequencies on probe diffraction pattern in the presence of the third-order susceptibility. Specifically, in Fig. 5 the probe laser frequency was fixed at Δ_p = 0 and investigated the variation of the probe diffraction pattern at different coupling laser frequencies Δ_c. Here, we have chosen the coupling detuning Δ_c = -15γ and +15γ, while the probe and coupling laser fields are ω_p = 1γ and ω_c = 30γ. It shows that when Δ_c = -15γ, the first-order diffraction intensity is enhanced at the angle sinθ = -0.25, while Δ_c = +15γ, the first-order diffraction intensity is enhanced at the angle sinθ = +0.25. To explain

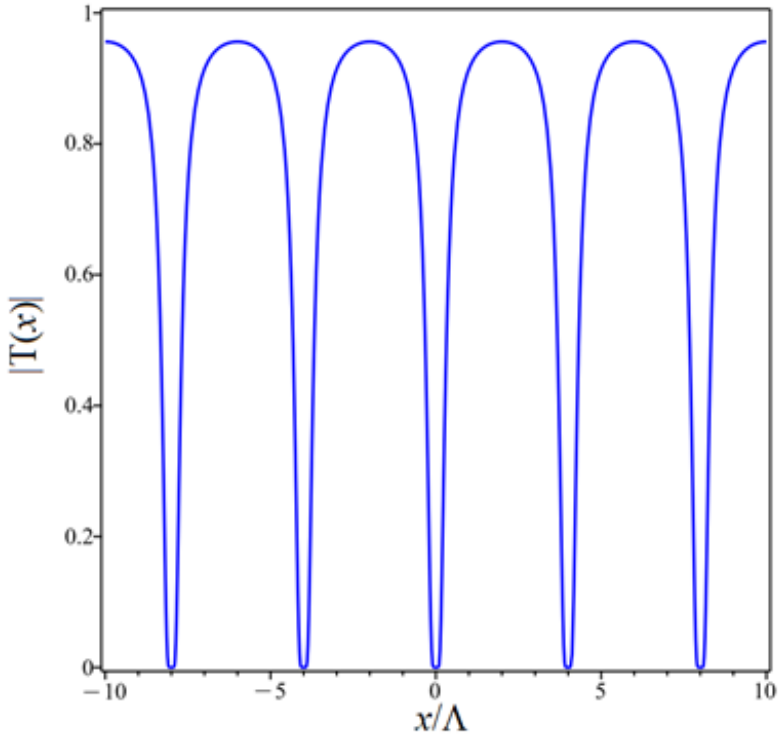

Fig. 3. Transmission function |T(x)| versus transverse position x. Employed common parameters as $\omega_p = 1\gamma$, $\omega_c = 30\gamma$, $\Delta_c = \Delta_p = 0$, M = 7, L = 15 and R = 4 ($\phi \approx 7.3^\circ$).

these phenomena, we plotted the absorption Im(ρ_{21}) and dispersion Re(ρ_{21}) at different coupling detunings $\Delta_c = 0$ (solid line), $\Delta_c = 15\gamma$ (dashed line) and $\Delta_c = -15\gamma$ (dash-dotted line), as shown in Fig. 6. We can see from Fig. 6 that by adjusting the coupling or probe frequency around the corresponding atomic resonance frequency, the position of the EIT window is moved away from the two-photon resonance position. Namely, the EIT-window position is shifted to the left when the coupling detuning is negative and it is shifted to the right when the coupling detuning is positive; the dispersion curves are also shifted accordingly, so that the dispersion amplitude is increased in the atomic resonance region $\Delta_p = 0$. Furthermore, it can be seen that at the two-photon resonance $\Delta_c = \Delta_p = 0$, the EIT is symmetric, but the symmetry of the EIT no longer remains when Δ_c is non-zero. Thus, the increase in dispersion leads to a phase modulation of the transmission function $T(x)$ that tends to disperse energy into higher-order maxima. Therefore, at $\Delta_c = \pm 15\gamma$ the phase diffraction pattern is formed in which there is a transfer of probe light energy from zero-order diffraction to first-order diffraction, as shown in Fig. 5. On the other hand, we can also easily see from Fig. 5 that in the presence of the third-order susceptibility, the first-order (and zero-order) diffraction efficiency is significantly larger than the case where the third-order susceptibility is ignored. Specifically, the first-order diffraction efficiency can be achieved as high as 16% with the third-order susceptibility, while it is only about 8% without the third-order susceptibility (i.e., about 50% larger). It is also a remark that the first-order diffraction plays a very important role in

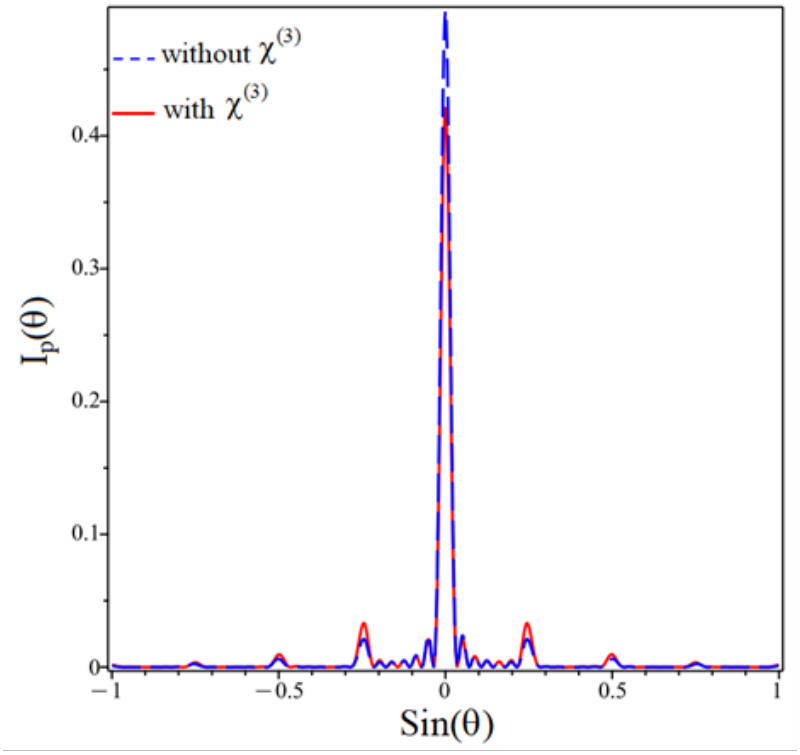

Fig. 4. Diffraction pattern of the probe field without $\chi^{(3)}$ (dashed line) and with $\chi^{(3)}$ (solid line) at the laser and medium parameters as $\omega_p = 1\gamma$, $\omega_c = 30\gamma$, $\Delta_c = \Delta_p = 0$, $M = 7$, $L = 30$ and $R = 4$ ($\phi \approx 7.3^{\circ}$).

applications of diffraction gratings, so it is always desirable to achieve high efficiency of first-order diffraction.

In Fig. 7, the coupling frequency is fixed at $\Delta_c = 0$ and the diffraction pattern is constructed at different values of $\Delta_p = 10\gamma$, and $\Delta_p = -10\gamma$. From the figure we see that when $\Delta_p = -10\gamma$, the first-order diffraction intensity is enhanced at the angle $\sin\theta = +0.25$, while $\Delta_p = +10\gamma$, the first-order diffraction intensity is enhanced at the angle $\sin\theta = -0.25$. This phenomenon is also explained similarly as that in Fig. 5, however, we also note that at $\Delta_p = \Delta_c = 0$ the absorption and dispersion are almost zero (see solid lines in Fig. 6), while at $\Delta_p = \pm 10\gamma$ the dispersion amplitude is significantly enhanced (absorption also increases but remains within the EIT spectral region). These lead to a phase modulation of the transmission function, such that the phase diffraction pattern is formed in which there is a transfer of probe light energy from zero-order diffraction to first-order diffraction. In this case, we can obtain diffraction efficiencies of 21% and 11% in the presence and absence of the third-order susceptibility, respectively.

4. Possible experimental realization

In an experiment, we can use the cold ^{85}Rb atom with the associated energy levels indicated in Fig. 8(a). The cold ^{85}Rb atoms can be obtained by a magneto-optical trap (MOT). The

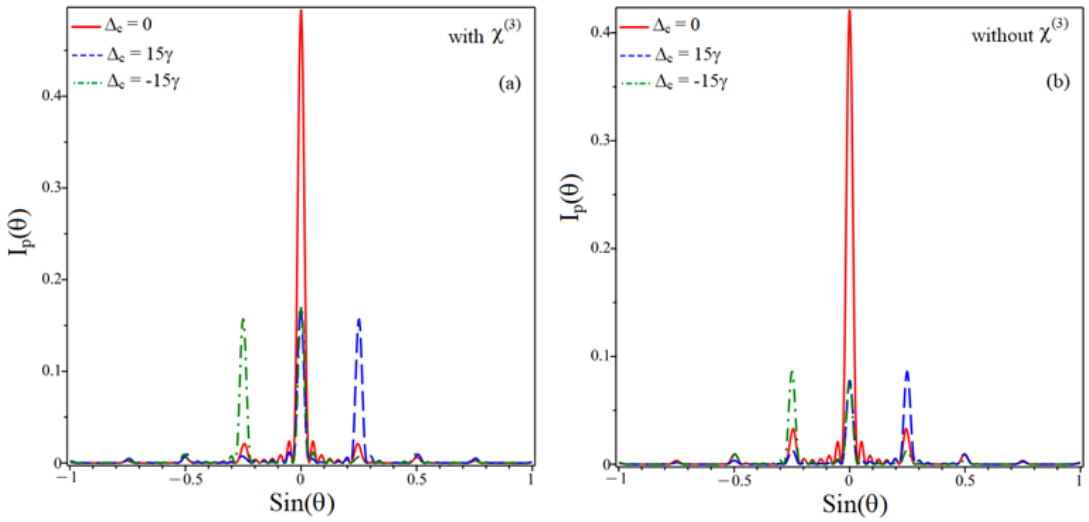

Fig. 5. The phase diffraction pattern of the probe beam at different coupling detunings [$\Delta_c = 0$ (solid line), $\Delta_c = 15\gamma$ (dashed line) and $\Delta_c = -15\gamma$ (dash-dotted line)] with $\chi^{(3)}$ (a) and without $\chi^{(3)}$ (b). The laser and medium parameters are used as $\omega_p = 1\gamma$, $\omega_c = 30\gamma$, $\Delta_p = 0$, $M = 7$, $L = 30$ and $R = 4$ ($\phi \approx 7.3^{\circ}$).

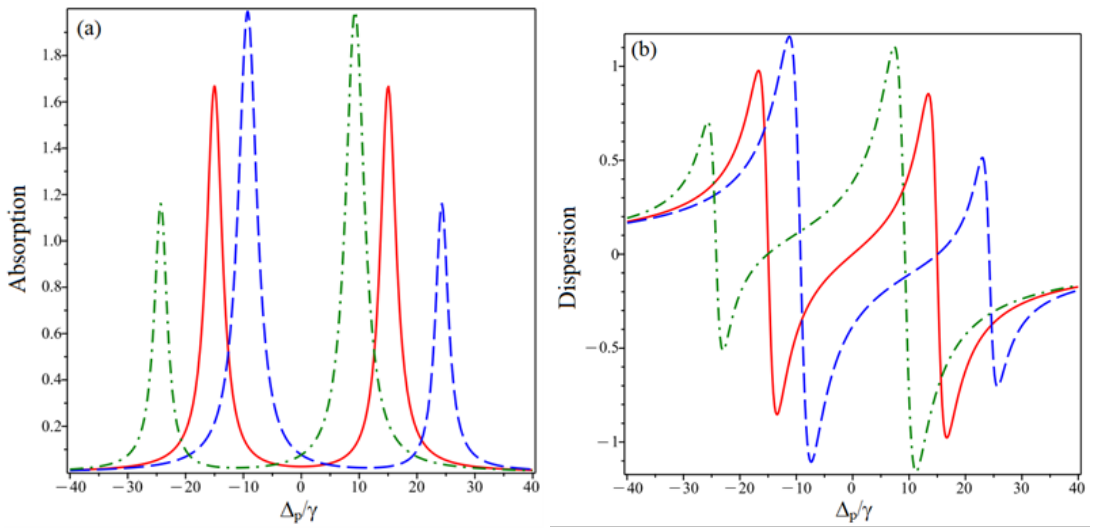

Fig. 6. (a) Probe absorption Im(ρ_{21}) and (b) dispersion Re(ρ_{21}) at different coupling detunings [$\Delta_c = 0$ (solid line), $\Delta_c = 15\gamma$ (dashed line) and $\Delta_c = -15\gamma$ (dash-dotted line)] with the prensence of $\chi^{(3)}$. Other parameters are $\omega_p = 1\gamma$, $\omega_c = 30\gamma$, $\Delta_p = 0$.

probe laser operating at the wavelength of 795 nm excites the atom from the ground state $5S_{1/2}$ $F = 1$ to the excited state $5P_{3/2}$ $F' = 2$. While the coupling laser operating at the wavelength of 780 nm pumps the atom from the ground state $5S_{1/2}F = 1$ to the excited state $5P_{1/2}F' = 2$. The

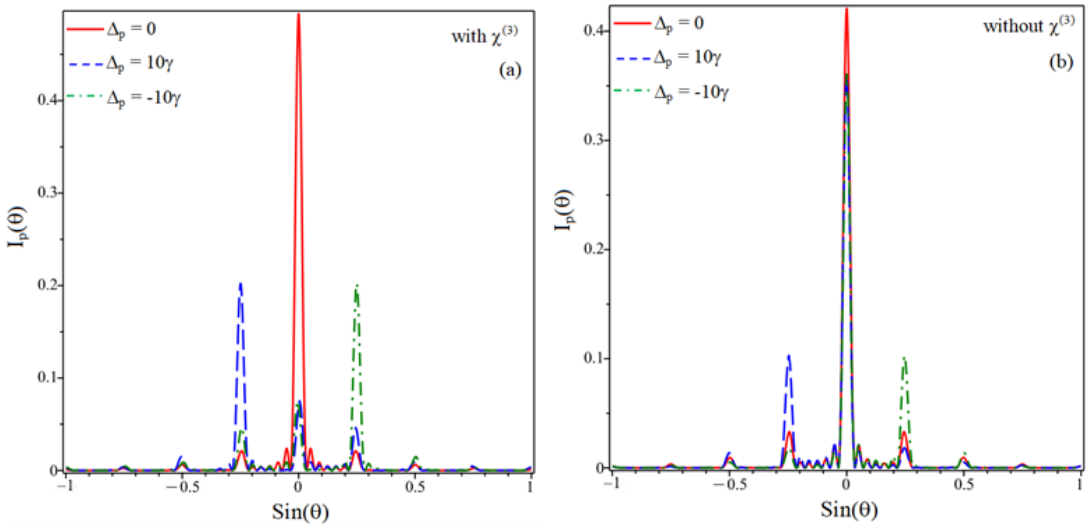

Fig. 7. (a) The phase diffraction pattern of the probe beam at different probe detunings [$\Delta_p = 0$ (solid line), $\Delta_p = 05\gamma$ (dashed line) and $\Delta_p = -10\gamma$ (dash-dotted line)] with $\chi^{(3)}$ (a) and without $\chi^{(3)}$ (b). The laser and medium parameters are used as $\omega_p = 1\gamma$, $\omega_c = 30\gamma$, $\Delta_c = 0$, $M = 7$, $L = 30$ and $R = 4$ ($\phi \approx 7.3^{\circ}$).

coupling and probe lasers are both continuous waves and can be provided by two external cavity diode lasers. The laser intensities can be adjusted by a neutral density filter (ND). We can use a polarization beam splitter to split the initial coupling beam into two beams, as shown in Fig. 8(b). The reflected coupling beam can be used for setting an EIT reference signal (not shown in figure). The transmitted coupling beam is transformed into an elliptical shape by using an anamorphic prism pair. Then, the two coupling beams with a small angle 2ϕ are recombined together in the center of the atoms ensemble to generate the standing-wave field whose period is determined to be $\Lambda = \Lambda_c/(2\sin\phi)$, where Λ_c is the wavelength of coupling laser. The laser frequencies can be detuned by a laser controller. The output of the probe beam can be imaged onto a CCD camera.

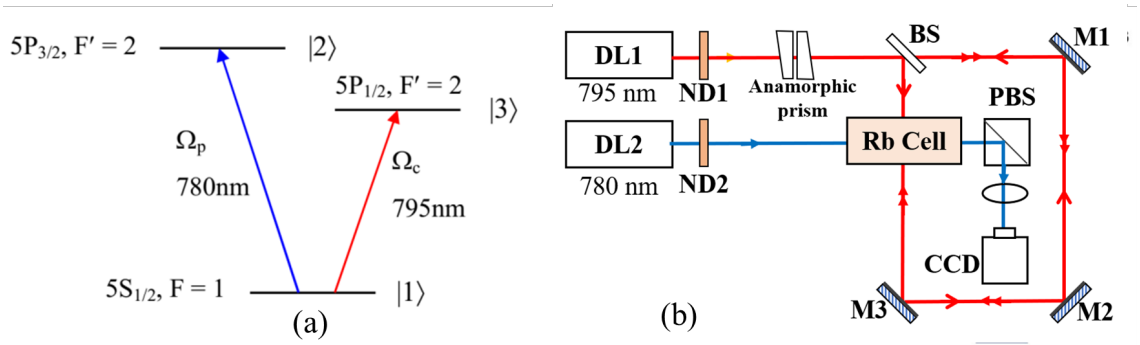

Fig. 8. (a) The three-level V-type scheme of ^{85}Rb atom. (b) Schematic diagram of experimental setup.

5. Conclusion

In this work, we have investigated the influence of the third-order susceptibility on electromagnetically induced grating in the three-level V-type atomic system. In the presence of the third-order susceptibility, the amplitude of the probe absorption is reduced, so that the EIG diffraction efficiency is also increased. Particularly, by changing the coupling or probe laser frequency around the atomic resonance frequency, the first-order diffraction efficiency is dramatically increased, i.e., there is a transfer of light energy from zero-order diffraction to first-order diffraction - this case corresponds to a phase grating. In this case, the first-order diffraction efficiency in the presence of the third-order susceptibility can be about 50% larger than that in the case of the third-order susceptibility is ignored. This study is necessary because the giant nonlinearity of the EIT material cannot be neglected even at very low light intensities, so the simulation results can be in better agreement with experimental observations.

Acknowledgment

This research was funded by Vietnam's Ministry of Education and Training under Grant No. B2023-TDV-08.

References

[1] N. Bonod and J. Neauport, *Diffraction gratings: from principles to applications in high-intensity lasers*, Adv. Opt. Photon. **8** (2016) 156.
[2] K. J. Boller, A. Imamoglu and S.E. Harris, *Observation of electromagnetically induced transparency*, Phys. Rev. Lett. **66** (1991) 2593.
[3] A. Lezama, S. Barreiro and A. M. Akulshin, *Electromagnetically induced absorption*, Phys. Rev. A **59** (1999) 4732.
[4] H. Ling, Y. -Q. Li and M. Xiao, *Electromagnetically induced grating: homogeneously broadened medium*, Phys. Rev. A **57** (1998) 1338.
[5] M. Mitsunaga and N. Imoto, *Observation of an electromagnetically induced grating in cold sodium atoms*, Phys. Rev. A **59** (1999) 4773.
[6] G. Cardoso and J. Tabosa, *Electromagnetically induced gratings in a degenerate open two-level system*, Phys. Rev. A **65** (2002) 033803.
[7] B. K. Dutta, P. K. Mahapatra, *Electromagnetically induced grating in a three-level Ξ-type system driven by a strong standing wave pump and weak probe fields*, J. Phys. B: At. Mol. Opt. Phys. **39** (2006) 1145.
[8] S. A. Carvalho and L. E. E. de Araujo, *Electromagnetically induced blazed grating at low light levels*, Phys. Rev. A **83** (2011) 053825.
[9] S. Asghar, Ziauddin, S. Qamar and S. Qamar, *Electromagnetically induced grating with Rydberg atoms*, Phys. Rev. A **94** (2016) 033823.
[10] J. W. Tabosa, A. Lezama and G. Cardoso, *Transient Bragg diffraction by a transferred population grating: application for cold atoms velocimetry*, Opt. Commun. **165** (1999) 59.
[11] D. Moretti, D. Felinto and J. W. R. Tabosa, *Dynamics of a stored Zeeman coherence grating in an external magnetic field*, J. Phys. B **43** (2010) 115502.
[12] L. Zhao, W. Duan and S. F. Yelin, *All-optical beam control with high speed using image-induced blazed gratings in coherent media*, Phys. Rev. A **82** (2010) 013809.
[13] J. Wen, Y. H. Zhai, S. Du and M. Xiao, *Engineering biphoton wave packets with an electromagnetically induced grating*, Phys. Rev. A **82** (2010) 043814.
[14] Y. Zhang, Zh. Wu, X. Yao, Zh. Zhang, H. Chen, H. Zhang and Y. Zhang, *Controlling multi-wave mixing signals via photonic band gap of electromagnetically induced absorption grating in atomic media*, Opt. Express **21** (2013) 29338.

[15] T. Qiu and G. Yang, *Electromagnetically induced angular Talbot effect*, J. Phys. B: At. Mol. Opt. Phys. **48** (2015) 245502.
[16] Gh. Solookinejad, M. Panahi, E. A. Sangachin and S. H. Asadpour, *Plasmonic structure induced giant Goos-Hänchen shifts in a four-level quantum system*, Chin. J. Phys. **54** (2016) 651.
[17] R. Sadighi-Bonabi, T. Naseri and M. Navadeh-Toupchi, *Electromagnetically induced grating in the microwavedriven four-level atomic systems*, App. Opt. **54** (2015) 368.
[18] N. Ba , X.-Y. Wu, X.-J. Liu, S.-Q. Zhang and J. Wang, *Electromagnetically induced grating in an atomic system with a static magnetic field*, Opt. Commun. **285** (2012) 3792.
[19] T. Naseri, R. Sadighi-Bonabi, *Electromagnetically induced phase grating via population trapping condition in a microwave-driven four-level atomic system*, J. Opt. Soc. Am. B **31** (2014) 2879.
[20] N. Ba, L. Wang, X.-Y. Wu, X.-J. Liu, H.-H. Wang, C.-L. Cui and A.-J. Li, *Electromagnetically induced grating based on the giant Kerr nonlinearity controlled by spontaneously generated coherence*, App. Opt. **52** (2013) 4264.
[21] H. Wang, D. Goorskey, and M. Xiao, *Enhanced Kerr nonlinearity via atomic coherence in a three-level atomic system*, Phys. Rev. Lett. **87** (2001) 073601.
[22] N. T. Anh, L. V. Doai and N. H. Bang, *Manipulating multi-frequency light in a five-level cascade-type atomic medium associated with giant self-Kerr nonlinearity*, J. Opt. Soc. Am. B **35** (2018) 1233.
[23] L. V. Doai, *Giant cross-Kerr nonlinearity in a six-level inhomogeneously broadened atomic medium*, J. Phys. B: At. Mol. Opt. Phys. **52** (2019) 225501.
[24] A. Hussain, M. Abbas and H.t Ali, *Electromagnetically induced grating via Kerr nonlinearity, Doppler broadening and spontaneously generated coherence*, Phys. Scr. **96** (2021) 125110.
[25] N. H. Bang, D. X. Khoa and L. V. Doai, *Review: Controllable optical properties of multi-electromagnetically induced transparency gaseous atomic medium*, Comm. Phys. **28** (2019) 1.